Monte Carlo simulation of a helium film on graphite

P. A. Whitlock
Department of Computer Science, Brooklyn College, Brooklyn, New York 11210

G. V. Chester and B. Krishnamachari
Laboratory of Atomic and Solid State Physics, Cornell University, Ithaca, New York 14853

(Received 24 March 1998)

Green's-function Monte Carlo and variational methods are used to calculate the properties of a monolayer of helium on a smooth graphite substrate. We find that in all respects these properties are very close to those of two-dimensional helium. There are small differences in the equations of state of the two systems. We use these results to show how accurate chemical potentials can be constructed for particles in the second and third layers and we compute the densities at which these layers will begin to form. These densities are in good agreement with the experimental values. [S0163-1829(98)08737-2]

I. INTRODUCTION

Helium four films on graphite substrates have been the subject of many experimental investigations.[1] Graphite provides an especially interesting substrate because of the relatively large areas which exist as well-defined crystal surfaces, each with a hexagonal arrangement of carbon atoms. The following phenomena for the film are well established. Helium is strongly absorbed and covers the substrate with a tightly bound monolayer. Upon addition of further helium, additional layers are formed in a well-defined manner; seven distinct layers have been observed.[2] In this simulation study we have focused in some detail on the properties of the first layer and have used these results to construct a simple model that allows us to study the formation of the second and third layers. Recently detailed studies of the superfluid properties of the second and third layers have been published.[3] Superfluidity has however not been seen in the first, and most tightly bound, layer. Experimentally, it seems to be well established that there are three distinct density regimes for the first layer.[2] At the very lowest coverages and at the lowest temperatures the helium probably condenses into nearly two-dimensional clusters and/or is preferentially absorbed onto step irregularities on the surface. At higher densities several commensurate phases exit. Beyond these, as the density increases, there is a third region in which an incommensurate triangular crystal is formed. The commensurate phases form because of the regular hexagonal arrangement of the carbon atoms in the substrate. When the density of the crystalline phase becomes sufficiently large, approximately 0.07 atoms Å^{-2}, the lowest energy state is that of the triangular helium lattice. In this state, the periodicity of the substrate plays a secondary role. At a density of approximately 0.11 atoms Å^{-2} the system starts to form a second, well defined, layer of helium atoms. These second layer atoms now see the dense incommensurate first layer as a substrate, modulated by the more distant carbon substrate. Again as the density of the second layer is increased, a second incommensurate triangular lattice is formed and at a slightly higher density the third layer begins to form.[2]

The first part of our work consisted of a detailed examination of the properties of the first layer. This layer is very tightly bound to the graphite substrate in a potential whose mean depth is approximately -180 °K. As a result the helium particles are confined within a profile determined by the ground-state wave function $\phi_0(z)$. Here z is the coordinate of a helium atom normal to the plane of the substrate; we show this wave function in Fig. 1. Since its width at half height is about 0.7 Å the helium atoms are essentially confined to a plane making very limited motion in the z direction. These facts are of course well known and have led to the very plausible suggestion that this first layer of helium will behave like two-dimensional (2D) helium.[4] This latter system was studied[5] some years ago and we thus have available accurate data with which to compare our film results. We are able to confirm the expectation that the properties of the first layer are very close to those of the 2D system. There are small, but significant, differences in the equation of state.

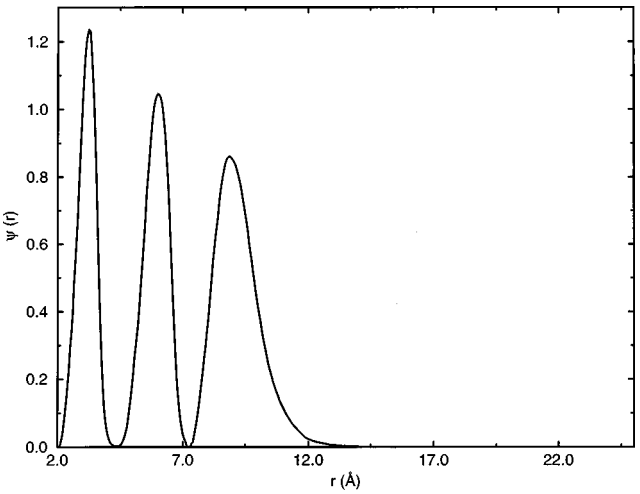

FIG. 1. The wave functions for the first, second, and third layers of helium on a graphite substrate. The functions are the eigenfunctions for the lowest state in the effective potentials which self-consistently allow for the presence of the other layers as discussed in the text. The density of the first layer is $\rho = 0.115\ \text{Å}^{-2}$, while that of the second layer is $\rho = 0.08\ \text{Å}^{-2}$. These are the densities at which the third layer starts to form.

The correlation functions and lattice displacements are essentially indistinguishable from those of the 2D system. We have used these results to make a simple model, based on the 2D equation of state to study the formation of the second and third layers. Both these layers are also similar to the 2D system. We predict that the second layer will crystallize just before completion.

There have been several other theoretical studies of helium films on graphite. Review of this work has been given by Clements *et al.*,[6] Gernoth, Clark, and Ristig,[7] and Saarela *et al.*[8] Progress has been made both at absolute zero and at finite temperatures. At absolute zero two methods have been used. The first is an optimized variational method (E-L HNC) which exploits the hypernetted chain formation (HNC) formalism together with Euler-Lagrange equations to compute the physical properties. It has been shown[9] that this method can give an accurate account of the ground-state properties of both the three-dimensional and two-dimensional homogeneous helium phases. Density-functional theory[10–12] has also been applied to helium films. This appears to be much less successful when compared with the optimized E/L HNC approach.[9] The successful E/L HNC work has been focused on the more weakly binding substrates; graphite covered with two solid layers of helium and the alkali metals. The focus of the work reported in this paper is different; the first two layers of helium on a graphite substrate. Our methods are also different; variational and Greens-function Monte Carlo. This approach is complimentary to the E/L HNC method and should provide useful data with which to test that kind of theory. A point in common in both approaches is the use and testing of a 2D model as an accurate approximation to describe a thin helium film.

Our first layer study is based on a simplified helium carbon interaction. We take this to be the mean interaction averaged across the substrate plane: it is thus a function of z alone. This model eliminates the commensurate phases which have experimentally been studied in detail. However we believe that apart from the elimination of these phases this model should be accurate enough to allow us to deal with the incommensurate solid phase and the properties of the second and third layers. In this model we find a homogeneous fluid at low densities, a two-phase coexistence with the triangular solid which increases significantly in density at the point of completion of the first layer. We have computed the equations of state of these phases, their correlations functions and have examined the relation between our model of the helium film and 2D helium.

In Sec. II we outline our computational methods. Section III describes our data for the first layer. In Sec. IV we describe methods by which effective potentials can be constructed for particles in the second and third layers. Section V is devoted to a discussion of the formation of the second and third layers. Our conclusions are in Sec. VI.

II. COMPUTATIONAL METHODS

In this study of the helium film we have used both the variational and exact Green's-function Monte Carlo (GFMC) methods. The optimized trial wave functions from the variational calculations are used as importance functions in the GFMC calculations. We will not provide a description of either of these methods. Detailed descriptions have been given in several places.[13,14]

The Hamiltonian for our system is given by

$$H=T+V+\sum_{i=1}^{N} V_0(z_i). \tag{1}$$

Here T and V are the kinetic and potential energies of N helium atoms. They are assumed to interact via a pairwise central potential. For this potential we have chosen that due to Aziz *et al.*,[15] which was used in studies of both bulk three-dimensional helium[16] and two-dimensional helium.[5] The potential energy, $V_0(z_i)$, is the potential felt by the ith atom due to the smooth carbon substrate. We used a form developed by Carlos and Cole[17]

$$V_0(z_i)=\left(\frac{4\pi\epsilon\sigma^6}{a_s d^4}\right)\left[\frac{2}{5}\left(\frac{\sigma}{d}\right)^6\zeta\left(10,\frac{z_i}{d}\right)-\zeta\left(4,\frac{z_i}{d}\right)\right] \tag{2}$$

with $\epsilon=16.24$ K, $\sigma=2.74$ Å, $d=3.37$ Å, and $a_s=5.24$ Å^2. $\zeta(n,z)$ is the generalized Riemann zeta function.[18] The coordinate z_i is normal to the substrate. We note that $V_0(z)$ is a much stronger potential than the Aziz potential. It has a depth of approximately -180 K compared with -10 K for the helium-helium potential.

Our variational wave functions, ψ_T, have the following forms. For the fluid phase

$$\psi_T=\Phi_J\Phi_3\Phi_S, \tag{3}$$

while for the solid phase

$$\psi_T=\Phi_J\Phi_3\Phi_S\Phi_G. \tag{4}$$

The functions appearing on the right-hand side of Eqs. (3) and (4) are defined by the following equations:

$$\Phi_J=\prod_{i<j}^{N}\exp[u(r_{ij})], \tag{5}$$

where

$$u(r_{ij})=[-1/2(b/r_{ij})^m]. \tag{6}$$

While one will get lower energies for the film using a shadow wave function,[19] we decided to use the same form as we had used in our study[5] of 2D helium so that we could make accurate comparisons between the two systems. Here b and m are variational parameters and r_{ij} is the distance between the ith and jth particles. Thus Φ_J is a Jastrow function with a MacMillan pseudopotential. The function Φ_3 describes correlations between triplets,[20]

$$\Phi_3=\exp\left[-\sum_{i<j}\overline{u}_{ij}-\frac{1}{2}\lambda_t\sum_k \mathbf{G}(k)\cdot\mathbf{G}(k)\right] \tag{7}$$

with

$$\tilde{u}_{ij}=u(r_{ij})-\lambda_t\xi^2(r_{ij})r_{ij}^2,$$

$$\mathbf{G}(k)=\sum_{i\neq k}\xi(r_{ij})\mathbf{r}_{ki},$$

and

TABLE I. The parameters, as defined in the text, for the optimized wave functions for the liquid (l), and solid (s) phases of the film. In the third column the symbol c defines the width of the Gaussian factors for the solid phase.

$\rho(\text{Å}^{-2})$	b(Å)	c	$\lambda_t(\text{Å}^2)$	s_t(Å)	ω_t(Å)	r_t(Å)
0.0321 l	3.042		−9.16	2.045	1.278	6.39
0.0421 l	3.067		−8.50	2.045	1.278	6.39
0.0536 l	3.144		−8.50	2.045	1.278	6.39
0.0612 l	3.144		−7.19	2.045	1.278	6.39
0.0689 l	3.144		−6.56	2.045	1.278	6.39
0.0689 s	2.888	0.306	−5.13	2.096	12.78	7.256
0.0765 s	2.863	0.383	−6.56	2.096	12.78	7.256
0.0842 s	2.863	0.459	−6.56	2.096	12.78	7.256
0.0918 s	2.863	0.612	−7.19	2.096	12.78	7.256
0.0995 s	2.837	0.689	−6.54	2.096	12.78	7.256

$$\xi(r_{ij})=\left(\frac{r_{ij}-r_t}{r_t}\right)^3\exp\left[\left(\frac{r_{ij}-s_t}{\omega_t}\right)^2\right],$$

where λ_t, s_t, ω_t, and r_t are variational parameters. The function Φ_S describes the localization of the atoms near the graphite substrate;

$$\Phi_S=\prod_{c=1}^{N}\phi_0(z_i), \tag{8}$$

and $\phi_0(z_i)$ is the ground-state wave function of a single helium atom interacting with the substrate via the potential $V_0(z_i)$, Eq. (2). We have solved this one-dimensional Schrödinger equation numerically. The lowest state has a sharp maximum at $z=2.9$ Å and a width at half height is approximately 0.7 Å. This is about 15% of the interparticle spacing in the film at the equilibrium density. Thus the particles are very tightly bound to the substrate and have very limited motion in the z direction. The eigenvalue E_0 corresponding to ϕ_0 is −140.74 K; we will refer to this as the single-particle ''binding energy,'' denoted by E_B. We have performed a Monte Carlo calculation of E_0, using ϕ_0 as a trial function and are able to reproduce the eigenvalue to six significant figures.

The function Φ_G is used only in the solid phase. It describes the localization of the particles in the neighborhood of the points of a plane triangular lattice.

$$\Phi_G=\prod_{i=1}^{N}\exp[-c/2(\mathbf{r}_i-\mathbf{R}_i)^2]. \tag{9}$$

Here c is a variational parameter and the $\mathbf{R}_i$ are the lattice vectors of a triangular lattice. The lattice spacing is determined by the density of the system. Our simulations were performed with between 64 and 100 particles. Periodic boundary conditions were used in the x and y directions. Since the particles are highly localized in the z direction it was unnecessary to apply periodic boundary conditions in this direction. From our description of the strong localization normal to the substrate, we suspect that the film will behave very like 2D helium and we therefore include comparisons with 2D simulations throughout our analysis. We have chosen to use a two-dimensional density to describe the state of the system; thus our unit of density is particles per Å^2.

III. THE FIRST LAYER

In this section we will present the results of our simulation studies for the first layer. We find, in general, that our results are very close to those of the 2D system. The only significant difference is that the helium film has a somewhat larger binding energy. This difference in binding energy grows larger at higher density. Since any phase transformations in the first layer depend critically on the energy, we have presented our equation of state results in some detail in subsection A. Subsection B gives a very brief summary of our results for the distribution functions, the density distribution normal to the substrate and the distribution of displacements from the lattice sites in the solid phase.

A. Equation of state for the first layer

A variational search was conducted to minimize the energy with respect to the parameters in the wave functions. For the fluid, either 64 or 81 particles were used. Simulations with 100 particles showed no difference within the small statistical errors. For the solid phase, 80 particles were used. The searches were carried out at five densities in each phase. These optimized functions were then used as importance functions in our GFMC simulations. Table I gives the optimum parameters for the fluid and solid; the parameter m, Eq. (6), has the value 5 for both phases. The values of the parameters in these two tables are close to those found for the wave functions for 2D helium.[5]

The equation of state for the fluid is shown in Fig. 2 and in Table II we give the values of both our variational and GFMC energies. The film energies have been normalized by subtracting the binding energy of a single helium atom to the substrate. In Fig. 2 we also show the equation of state for the 2D system and we see that at all densities they are close. The small differences increase with density. We have covered a very wide range of densities, from zero pressure to a metastable fluid just above the freezing density. In the last column of Table II we give the difference between the GFMC energies for the film and the 2D system. At all densities the film has a lower binding energy; 5% lower at the lowest density; 10% lower at the highest density. The small differences that we find are in disagreement with the only other variational Monte Carlo data that we are aware of. Using a different

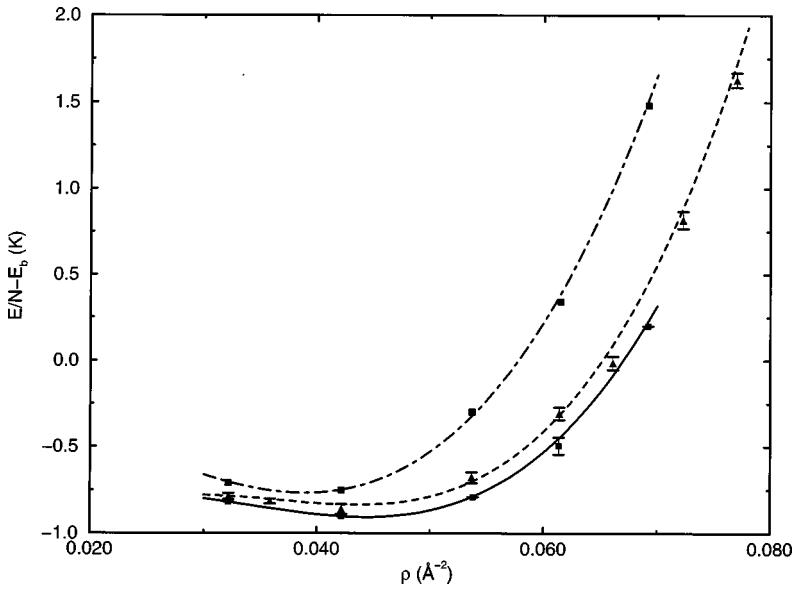

FIG. 2. The equation of state in the fluid phase. The solid curve is fitted to the GFMC data (boxes with error bars). The dashed line is fitted to the 2D GFMC data (triangles with error bars). The dashed-dot line is fitted to the variational film data (upper boxes).

two-body pseudopotential and a somewhat different helium-carbon potential Brami *et al.*[21] find a difference in energy between the film and the 2D system at a density 0.04 Å^{-2} of approximately -1.0 K. Their 2D energy is fairly close to ours, -0.9 K, however their film energy is much deeper -1.9 K. Using their two-body pseudopotential and the same helium carbon potential we have been unable to reproduce their results. We find a film energy of -0.73 K, which is close to the value shown in Table II.

The variational and GFMC energies were fitted to polynomials in the density ρ of the form

$$E = E_0 + B\left(\frac{\rho-\rho_0}{\rho_0}\right)^2 + C\left(\frac{\rho-\rho_0}{\rho_0}\right)^3. \tag{10}$$

We thus have four parameters to determine E_0, ρ_0, B, and C, from our five data points. We have chosen this form because we expect a minimum to occur in the energy as a function of density ρ; this minimum occurs at ρ_0 with a value of E_0, and corresponds to the fluid in equilibrium under zero pressure. Table III gives these parameters for both sets of data, variational and GFMC.

In Fig. 3 and in Table II we show the numerical values of both our variational and GFMC work for the triangular solid. The comparison between the data is very similar to that of the fluid phase. In the figure we compare the GFMC film results with the 2D GFMC solid.[5] Again we see that the film always has a lower energy and that the difference increases with increasing density. At the lowest density the difference is 0.12 K; rising to 1.00 K at the highest density.

The data for the solid was fitted to the same polynomial form as Eq. (10). The parameters, as determined from our fits, are given in Table III. The two equations of state were used to locate the melting and freezing densities using the Maxwell double tangent construction. In Fig. 4, we show the two GFMC equations of state and the double tangent construction. Table IV gives the values of the melting and freezing densities, for both the variational and GFMC equations of state. These densities are also given for the 2D system.

From the table we see that the melting and freezing densities obtained from our variational calculations for the film

TABLE II. The film and 2D energies for the liquid (l) and solid (s) phases. E_{var} is the variational energy, E_{GFMC} is the exact Green's-function energy, $E_{\text{GFM}}-E_B$ is the energy of the film minus the binding energy of a single helium atom on the carbon substrate, $E_{2\text{D}}$ is the GFMC energy of the 2D system, and Δ is the difference between the film energy (column 4) and that of the 2D system.

$\rho(\text{Å}^{-2})$	E_{var}(K)	E_{GFMC}(K)	$E_{\text{GFMC}}-E_B$	$E_{2\text{-}D}$(K)	Δ(K)$_{\text{(Film-2D)}}$
0.0321 l	-141.44 ± 0.02	-141.556 ± 0.005	-0.818 ± 0.005	-0.78 ± 0.02	-0.04 ± 0.02
0.0421 l	-141.49 ± 0.02	-141.64 ± 0.01	-0.90 ± 0.01	-0.85 ± 0.03	-0.05 ± 0.03
0.0536 l	-141.04 ± 0.04	-141.53 ± 0.01	-0.79 ± 0.01	-0.67 ± 0.03	-0.12 ± 0.03
0.0612 l	-140.42 ± 0.02	-141.23 ± 0.05	-0.49 ± 0.05	-0.30 ± 0.04	-0.19 ± 0.06
0.0689 l	-139.26 ± 0.04	-140.546 ± 0.009	0.192 ± 0.009		
0.0689 s	-139.97 ± 0.01	-140.42 ± 0.02	0.31 ± 0.02	0.43 ± 0.03	-0.12 ± 0.03
0.0765 s	-139.11 ± 0.02	-139.73 ± 0.01	1.01 ± 0.01	1.30 ± 0.02	-0.29 ± 0.02
0.0842 s	-137.735 ± 0.005	-138.50 ± 0.03	2.24 ± 0.03	2.78 ± 0.07	-0.54 ± 0.08
0.0918 s	-135.64 ± 0.02	-136.39 ± 0.02	4.35 ± 0.02	4.91 ± 0.03	-0.56 ± 0.03
0.0995 s	-132.61 ± 0.03	-133.42 ± 0.02	7.32 ± 0.02	8.26 ± 0.04	-0.94 ± 0.04

TABLE III. The equation-of-state parameters as defined in Eq. (10) for the liquid (l) and the solid (s) phases of the film.

Parameter	Variational	GFMC
$\rho_0(\text{Å}^{-2})$ l	0.0389±0.0005	0.0443±0.0005
E_0(K) l	−0.767±0.016	−0.906±0.009
B(K) l	2.418±0.35	1.956±0.10
C(K) l	1.722±0.42	2.904±0.42
χ^2/v of fit l	0.6515	0.374
$\rho_0(\text{Å}^{-2})$ s	0.0558±0.0003	0.0561±0.0005
E_0(K) s	0.3343±0.018	−0.0069±0.028
B(K) s	5.927±0.36	3.615±0.53
C(K) s	8.664±0.25	11.23±0.47
χ^2/v of fit s	5.755	5.143

and the 2D system are very similar. The most striking feature being that the difference $\Delta\rho=\rho_s-\rho_l$ is about twice as large in the film as the 2D system. However when we examine the two sets of GFMC data we see that this large difference in $\Delta\rho$ is no longer present. Only one small difference remains; there is about a 3% difference in the freezing densities. It is reasonable to place more weight on the GFMC data. Differences in the variational data can readily be attributed to differences in the ''goodness'' of the two wave functions. We therefore conclude that the melting and freezing of the incommensurate solid for the film takes place at almost the same densities found for the 2D system.

The GFMC melting density for the triangular solid film is 0.0724 particles per Å^{-2}. Unfortunately the value cannot be directly compared with data on the incommensurate solid on graphite. This solid phase is in equilibrium with a commensurate phase of some kind. Hence its transformation density need not be close to the melting density of the triangular solid on a smooth graphite substrate. Nevertheless it is worth pointing out that Greywall's data[2] suggests that the transition to the incommensurate phase takes place in the range 0.07 to 0.08 particles per Å^{-2}; our transition also lies in this range.

We now suggest a simple explanation for why the film is somewhat more bound than the 2D system. Whenever the density of liquid in solid helium decreases the energy of the system decreases. This is clearly seen for both the film and the 2D system from Figs. 2 and 3. It is equally true for three-dimensional helium. The underlying reason for this is however somewhat subtle. First we observe that when the density is decreased the potential energy becomes less negative. As the density decreases the mean distance between the particles increases and they move farther out on the attractive tail of the potential thus decreasing the magnitude of the negative potential energy. Thus the change in the potential energy will always tend to increase the total energy. However, whenever we decrease the density the kinetic energy decreases and by a larger amount than the change in the potential energy. The increase in mean distance between the particles means that the curvature of the wave function decreases because the function has more space in which to bend so that it vanishes on the ''hard core'' of the helium atoms. In both two and three dimensions the decrease in the kinetic energy, for a given decrease in density, is a good deal larger than the increase in potential energy. Hence the total energy always decreases. These observations can provide a simple explanation for the sign of Δ, the difference in energy of the film and the 2D system. We only have to notice that at the same areal density the particles in the film are at a slightly lower total density than those in the 2D system. This is because the small motion in the z direction means they are on the average further apart than those in the 2D system. We thus expect the potential energy to increase and the kinetic energy to decrease by a larger amount thus leading to negative values for Δ.

TABLE IV. The melting and freezing densities of the film and 2D system. All of these have been calculated from the appropriate equations of state by the Maxwell double tangent construction.

Method	$\rho_l(\text{Å}^{-2})$	$\rho_s(\text{Å}^{-2})$
Variational-Film	0.0537	0.0677
Variational-2D	0.0569	0.0642
GFMC-Film	0.0656	0.0724
GFMC-2D	0.0678	0.0721

Cheng, Cole, and Shaw[22] evaluated an approximate expression for Δ, the difference in binding energy of the film and 2D helium. Explicitly

$$\Delta \simeq \frac{\rho\langle z_{12}^2\rangle}{2}\int d^2r\; g(r)\;\frac{V'(r)}{2r}. \tag{11}$$

Here ρ is the density of the film, $\langle z_{12}^2\rangle$ is the expectation value of $(z_1-z_2)^2$ taken with respect to the product $\phi_0(z_1)\phi_0(z_2)$, and $g(r)$ is the two-dimensional pair-distribution function at the density ρ. The integral on the right-hand side of this equation is however difficult to evaluate. This is because the product of the distribution function $g(r)$ and $V'(r)/r$ is a very rapidly varying function for small r. If one uses tabulated values for $g(r)$, they are not accurate enough at small r to get the correct sign for Δ. However a direct calculation can be performed using configurations from a simulation of the 2D system. This leads to values for Δ with the same sign as those in Table II but somewhat smaller in magnitude.

B. Distribution functions

At each of the five densities in the fluid and solid phases we computed the pair-distribution function, and the density distribution normal to the substrate. The pair-distribution function was defined in terms of the projected positions of the particles onto a plane $z=$const. This definition allows an immediate comparison with the same function for 2D helium. We found that these pair-distribution functions are essentially identical with those found in 2D helium, at all densities in the fluid and solid phases. Figure 5 shows this comparison at the highest density in the solid. This confirms the expectation that the first layer of the film on graphite is a very two-dimensional system.

The distribution of atoms normal to the substrate is, at all densities, indistinguishable from the square of the ground-state wave function ϕ_0, see Fig. 1. This is not surprising as the binding energy in the potential well provided by the graphite is very much larger than the kinetic energy due to the lateral motion and the helium-helium interaction poten-

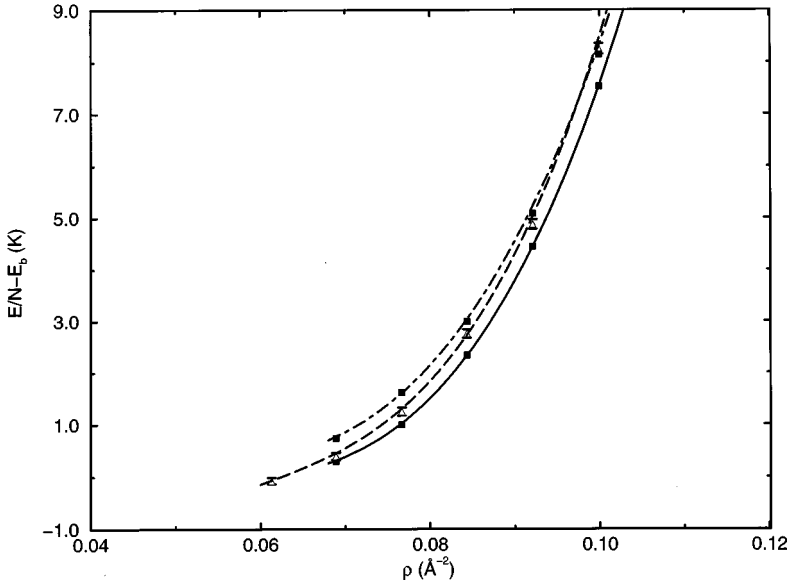

FIG. 3. The equation of state in the solid phase. The solid curve is fitted to the GFMC data (lower boxes). The dashed line is fitted to the 2D GFMC data (open triangles) and the dashed-dotted line is fitted to the film variational data (upper boxes).

tial. We conclude that even at the highest densities, where the second layer starts to form, the density profile of the first layer remains unaltered.

We have also computed the distribution of displacements of the helium atoms from their sites in the triangular lattice. The displacements in the direction normal to the substrate are much smaller than those in the plane of the film. These normal displacements are determined by the width of the ground-state wave function ϕ_0. The distribution of displacements in the plane of the film is very accurately a gaussian. The values of the moments of this Gaussian are the same, within our statistical uncertainties, as those we found in the 2D solid. Thus the triangular solid in the first layer is very like the 2D triangular solid except for small displacements out of the plane of the lattice. At the completion density of the first layer both the 2D and film systems are becoming close to harmonic. The mean-square displacements in the plane, from the lattice sites, are about 6% of the square of the near-neighbor distance. At the melting point of the triangular lattice the corresponding value is about 25%.

IV. CHEMICAL POTENTIALS AND EFFECTIVE POTENTIALS

It is well known that helium binds to graphite in successive layers. In this section we will suggest a simple model which allows one to compute the chemical potential of each layer accurately. The equilibrium between the layers is then determined by equating their chemical potentials. We use this to study the formation of the second and third layers.

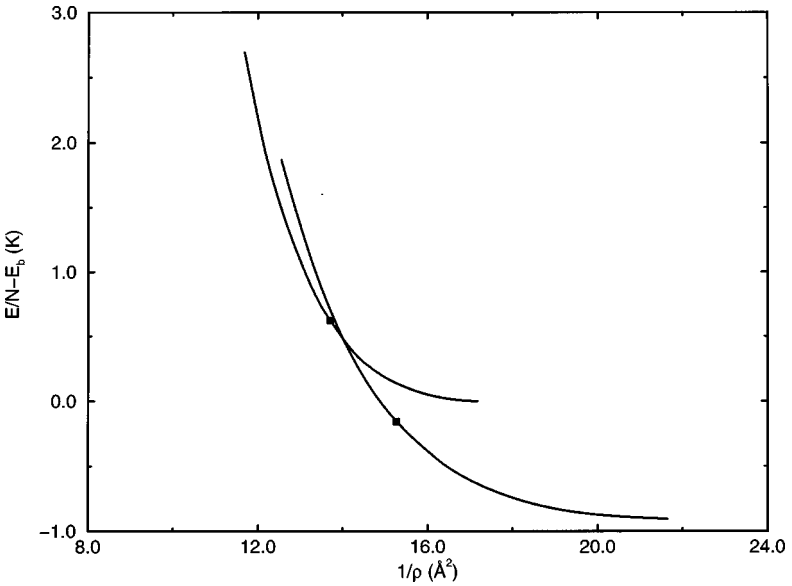

FIG. 4. The film GFMC energies for both the fluid and the solid versus $1/\rho$. The boxes represent the points of contact in the double tangent construction and locate the melting and freezing densities.

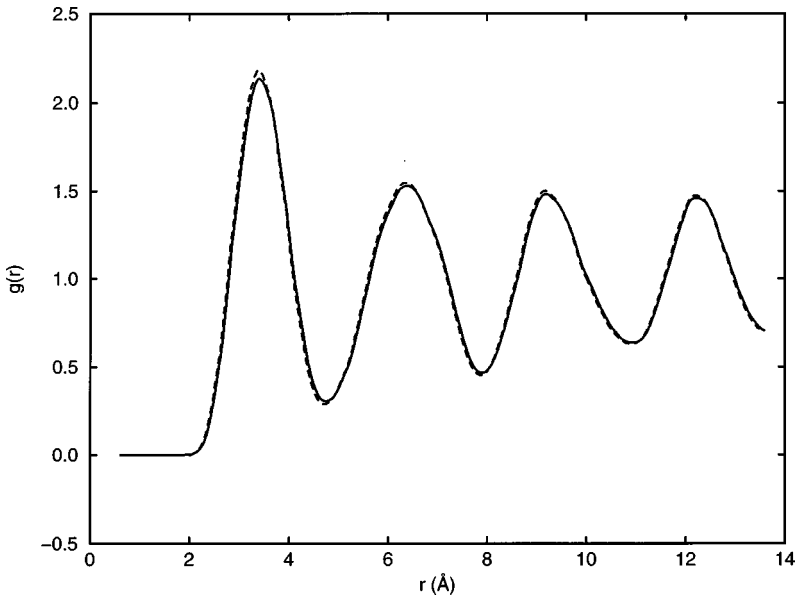

FIG. 5. The radial distribution function in the plane of the film and that of the 2D system. The solid curve is for the 2D system, the dashed curve is for the film. Both are at a density $\rho = 0.0995$ Å^{-2}.

The chemical potential in any layer is given by

$$\mu(\rho) = E(\rho) + \rho \frac{dE(\rho)}{d\rho}. \tag{12}$$

Here $E(\rho)$ is the energy per particle at density ρ and the second term in Eq. (12) is the pressure term in the Gibbs free energy for particle. For the first layer we have accurate GFMC calculations that give us $E_1(\rho)$, hence we can immediately calculate μ_1 from Eq. (12). However we also have available an accurate approximation to $E_1(\rho)$; namely

$$E_1(\rho_1) \simeq E_{10}(H,C) + E_{2D}(\rho_1), \tag{13}$$

where E_{10} is the binding energy of a single helium atom to the carbon substrate and $E_{2D}(\rho_1)$ is the energy of the 2D helium system. We shall see that we do not need very accurate approximations for μ to determine the densities at which the second and third layers form. The two terms in Eq. (13) are quite different in character. The second term refers only to the particle interactions in the plane of the film, while the first term refers only to the interaction of a helium atom with the external potential; for the first layer this is the carbon potential. We now turn to the second layer and for the moment consider the situation when it has just formed and is thus very dilute. The appropriate form of our basic approximation is now

$$E_2(\rho_2;\rho_1) \simeq E_{20}(C,\rho_1) + E_{2D}(\rho_2). \tag{14}$$

E_2 and E_{20} will depend parametrically on ρ_1 because the binding energy of a helium atom in the second layer depends on both the carbon potential, now at some distance away, and the potential provided by the first layer at a density ρ_1.

The second, and final, step in our approximate method is to show that a very simple approximation allows us to calculate $E_{20}(C,\rho_1)$ with sufficient accuracy. We compute E_{20} by constructing an effective external potential for the particles in the second layer. We should however make it clear that a precise calculation of E_{20} cannot be performed in terms of an external static potential. This is because the presence of atoms in the second layer influences those in the first layer. The effective potential approximation does not take this effect into account. However, as long as the first layer is a dense solid it is very plausible that the influence of the atoms in a dilute second layer will be small. We will return to this point later. Our effective potential for a helium atom in the second layer consists of two parts, that provided by the carbon substrate and that due to the interaction with the atoms in the first layer. The carbon substrate potential is of course known, at the position of the second layer it is rather slowly varying with a value of ~ -23 K. The effective potential provided by the first layer can be calculated exactly. At any point (x,y,z) in the second layer there is a potential $V_E(x,y,z;R)$, where R refers to a particular configuration of atoms in the first layer. Explicitly

$$V_E(x,y,z;R) = V_E(\underline{r};R) = \sum_{j=1}^{N} V(\underline{r} - \underline{r}_j). \tag{15}$$

Here V is the Aziz potential between two helium atoms and r_j is the position of the jth atom in the first layer. We now average over the configurations of the first layer by taking the expectation value of V_E with respect to the ground-state wave function $\Psi_0(R)$ for the first layer; the effective potential $\overline{V}_E$ is thus given by the equation,

$$\overline{V}_E(r) = \langle V_E(r;R) \rangle = \int \Psi_0^2(R) V_E(r;R) dR. \tag{16}$$

We can perform this average by using our GFMC configurations; and we can therefore compute $\overline{V}_E$ as a function of density of the first layer. We will refer to $\overline{V}_E$ as the exact effective potential. We expect the first layer to be a triangular solid when the second forms, and therefore $\overline{V}_E(x,y,z)$ will exhibit, in x and y, the periodicity of this lattice. We will use this effective potential to provide bounds on the chemical potential of the dilute second layer.

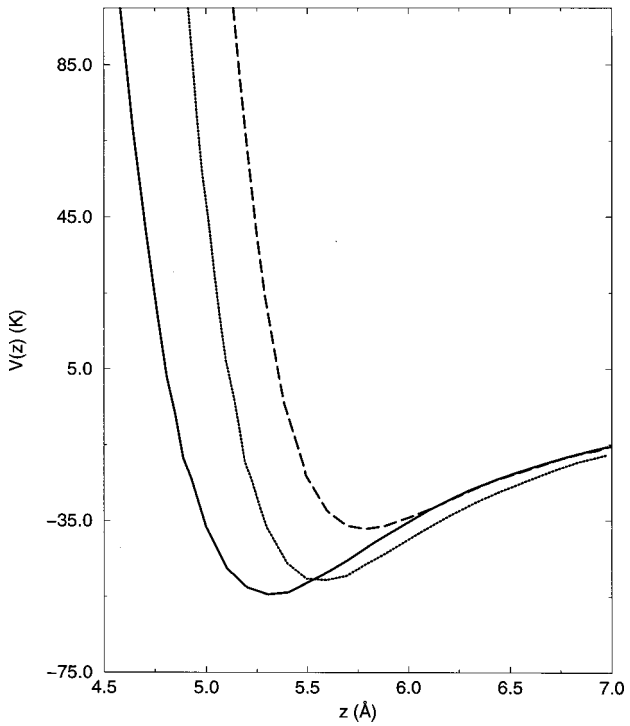

FIG. 6. Potential energy curves for an atom in the dilute second layer. $V_{\max}(z)$ (— — —) is the potential which bounds $V_E(x,y,z)$ above for all (x,y): $V_{\min}(z)$ (——) is the potential which bounds $\overline{V_E}(x,y,z)$ below for all x,y. $\tilde{V}_E(z)$ (· · · ·) is the mean Aziz potential defined in the text.

This effective potential is, as we have pointed out, a periodic function of x and y. We will find it useful to make a further approximation so that our effective potential is independent of x and y and thus depends only on z. This kind of approximation leads to rather small errors in our estimates of the densities at which the second and third helium layers form. We chose the simplest approximation to $\overline{V_E}$. For the layers which are relatively tightly bound we assume that the atoms are confined to a plane. The effective potential seen by an atom in any other layer is then computed by integrating $\overline{V_E}(r)$, Eq. (16), across the plane. This removes the x,y dependence and we have a potential $\tilde{V}_E(z)$ which depends parametrically on the density of the atoms in the plane. This is a very simple approximation and is in the same spirit as our approximation in which we replace the film energy with the energy of the 2D system. These two approximations form the basis of our calculations.

In Fig. 6 we show three potential curves as a function of z. The curve with the highest energy is $\overline{V_E}(x,y,z)$ when x,y are held fixed above an atom in the triangular lattice. The lowest energy curve is $\overline{V_E}(x,y,z)$ when x,y are held fixed at the center of one of the triangles of the lattice. The curve that lies between these is our simplified effective potential $\overline{V_E}(z)$. In the Appendix we show that the lowest eigenvalue of the exact effective potential, $\overline{V_E}(r)$, lies between the lowest eigenvalues of the upper and lower potentials as we have defined them. Since the minimum of $\tilde{V}_E(z)$ is bounded by the minimum of $V_{\max}$ and $V_{\min}$ its lowest eigenvalue will also lie between these bounds. We are thus confident that the lowest eigenvalue of $\tilde{V}_E(z)$ is an accurate approximation to the lowest eigenvalue of $\overline{V_E}(x,y,z)$. We will therefore use this approximate effective potential to discuss the formation of the second and third layers.

V. LAYER COMPLETION AND FORMATION

We first present the results of our calculations for the density of formation of the second layer. We use the bounds discussed above to bound the chemical potential of the second layer and we use our GFMC results to compute the chemical potential of the first layer. We then compare this result with those obtained from our 2D approximation.

The density at which the second layer will form is given by the solution to the equation

$$\mu_2(\rho_2;\rho_1)=\mu_1(\rho_1)=E_1(\rho_1)+\rho_1\frac{dE_1}{d\rho_1}. \tag{17}$$

When the second layer first forms it will be dilute and the dependence of μ_2 on ρ_2 can be neglected, and $\mu_2(\rho_1)=E_2(\rho_1)$, the binding energy of a single particle in the presence of the crystalline first layer and the carbon substrate. The effective potential provided by the first layer depends on the density of that layer. The energy $E_1(\rho_1)$ is the energy of the film obtained from our GFMC calculations. In Fig. 7 we plot these two eigenvalues as a function of ρ_1. They decrease slowly as a function of ρ_1. We also plot the chemical potential of the first layer obtained from our GFMC calculation;[23] it intersects the eigenvalues at densities of 0.115 and 0.118 Å^{-2}. We can thus rigorously state that within the effective potential approximation the second layer will begin to form at a density lying between these bounds. On the same figure we have also plotted the eigenvalue corresponding to the mean potential $\tilde{V}(z)$. This predicts a formation density of 0.115 Å^{-2}. The density at which the first layer completes and promotion to the second begins has been determined by heat capacity, third sound and neutron-scattering measurements. These experiments do not appear to be in precise agreement, the values for the completion density range from 0.11 to 0.12 Å^{-2}.[24] Our values lie in this range. We note that the difference in our two bounds is less than 3%, which is smaller than the differences in the experimental results. However, we do not wish to place too much emphasis on the accuracy of our present work. It is based on four assumptions, each of which requires careful examination before one can claim great accuracy.

The first is the use of the earliest Aziz two-body potential.[15] This has now been superseded by more accurate potentials.[25] We chose to work with the older Aziz potential because our earlier 2D work had been done with that potential and were thus able to make interesting comparisons between the film and the 2D system. We have carried out GFMC calculations at the two highest densities, 0.11 and 0.12 Å^{-2} with one of the most recent Aziz potentials.[25] We find only a very small change in the energy of the film and hence no significant change in our estimates of the completion density. Second, we have ignored any contributions from three-body terms in the interaction potential. The Axilrod-Teller potential is known to give significant contributions to energy of a dense three-dimensional helium crystal.[16,26] We have made a simple estimate of the contri-

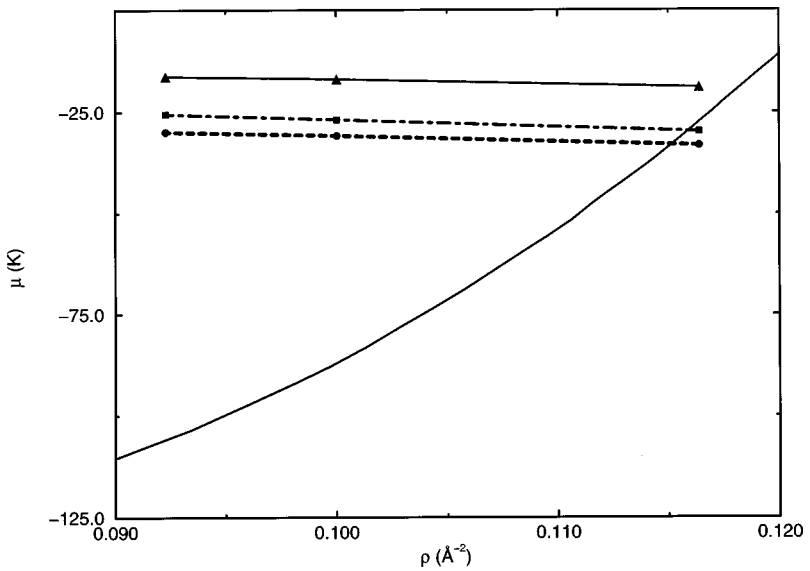

FIG. 7. The chemical potentials of the second layer and first layers. The three chemical potentials of the second layer have been calculated using the potentials $V_{\max}$ ($\cdot\ \cdot\ \cdot$), $V_{\min}$ ($-\ -\ -$), and $\tilde{V}_E$ ($—\ .\ —\ .\ —\ .\ —$). The chemical potential of the first layer (——) was calculated from the GFMC equation of state.

bution of this potential in the high density range of the solid first layer. This is based on a static lattice model,[27] and we find contributions to the chemical potential of the film of approximately +3.0 K. This change in μ leads to an increase of about 1% in our estimates of the density at which the first layer will complete. Third we have replaced the periodic potential of the carbon substrate with an averaged mean potential. Estimates[28] of the binding energy of the film on a corrugated carbon substrate suggest that it differs by about 0.01 K from that on a plane substrate.[29] This small charge will have no appreciable effect on the completion density. The corrugations of the carbon potential have become very small at the distance of the second layer and again will have no appreciable effect on the chemical potential of the second layer. Finally, as we have already pointed out, we have used an effective potential approximation to calculate the chemical potential of the second layer. We are able to check this assumption. We have available the results of computing the chemical potential of the dilute second layer by path-integral methods. Using this method we simulated the dense first layer in the presence of a single second layer atom without using any effective potential approximation. By the method we found a value of −29.8 K for the chemical potential of the dilute second layer. Our bounds for the chemical potential based on the effective potential $\tilde{V}_E$ are −30.1 and −19.6 K. The path-integral value lies in this range and we therefore conclude that for the second layer the effective potential approximation provides an accurate description. The basic reason for this is that at completion the first layer is an extremely dense solid and cannot be readily perturbed by atoms in the second layer. This argument does not apply so convincingly to an effective potential for atoms in the third layer. At completion the second layer has only just solidified and is therefore more likely to be perturbed by atoms in the third layer.

It is worth noting that these completion densities, ranging from 0.11 to 0.118, imply that the first layer is an extremely dense system when the second layer begins to form. As several authors have noted the melting density of the incommensurate solid first layer (0.07 Å^{-2}) is almost the same as that of the basal plane of the 3D hcp ^{4}He crystal at its melting density. Thus at this density we are in a familiar density range. However the completion densities are 60 to 70 % higher than the melting density. In 3D this is much higher than any density at which simulations have been done. As we have already noted the film has become close to a harmonic solid at these densities.

We can now use these results to test the two-dimensional approximation in which the equation of state of the first layer is replaced by the equation of state of 2D helium in the presence of the carbon substrate and the chemical potential of the dilute second layer is computed from an effective potential provided by a 2D crystalline first layer. From our previous work on the 2D helium system we have an accurate equation of state and can thus compute the chemical potential. For the effective potential for the second layer we have chosen to use the mean potential provided by the 2D crystalline layer. This corresponds to integrating the Aziz potential across the plane of the second layer, and is the 2D analog of the mean potential we used for our previous calculation. Figure 6 shows that this 2D mean potential is close to the film mean potential, suggesting that this approximation is accurate. These approximate chemical potentials intersect at a density of 0.111 Å^{-2}, which is outside the bounding densities of the previous calculation but which is within the range of experimental values. This type of 2D approximation was introduced by Campbell and Schick[29] and their results are close to ours, although they used several simplifying assumptions and in addition used the Lennard-Jones potential for helium. At that time the modern Aziz potentials were not available.

Since this rather simple approximation leads to satisfactory results it is natural to ask whether we can use it to determine the densities at which subsequent layers will form. We believe that the effective potential approximation will be accurate as long as the layers are well separated. That is as

long as the density profiles, or wave functions do not overlap appreciably. However, as we move farther and farther away from the carbon substrate the layers will be less tightly bound and will inevitably begin to overlap appreciably. Again as long as we are dealing with tightly bound layers we should be able to approximate them accurately with 2D systems. However, we need to go beyond this simplified picture. It is easy to see, and it is well established experimentally, that as the density of the second layer increases towards completion the density of the first layer also increases. It is therefore incorrect to treat the first layer as an entirely passive source of an effective potential for the second layer. As the second layer becomes more dense the pressure starts to rise rapidly and consequently its chemical potential also starts to rise. However, if the second layer is to be in equilibrium with the first layer its chemical potential must also rise. The only way this can come about is for its density to increase. Thus as we increase the total coverage sufficient atoms go into the first layer so that its chemical potential increases to maintain equality with the chemical potential of the second layer. To determine this increase in a fully self-consistent fashion would require a difficult simulation in which atoms are inserted and removed from the dense first layer. However, this can be avoided if we simply assume that the density of the first layer is unknown and determine it from the equation for the equality of the chemical potentials. For example, given the density ρ_2 of the second layer we can write

$$\mu_1(\rho_1;\rho_2)=\mu_2(\rho_2;\rho_1). \tag{18}$$

It is important to note that μ_2 depends parametrically on ρ_1, and that μ_1 depends parametrically on ρ_2. This comes about because the effective potential for particles in each layer depends on the density of the other. Hence for a given ρ_2, Eq. (18) can be solved for ρ_1.

With these preliminary remarks in mind we now use our 2D model to determine the density of the first and second layers at which the third layer starts to form. We have to find ρ_1 and ρ_2 which satisfy the two equations

$$\mu_1(\rho_1;\rho_2)=\mu_2(\rho_2;\rho_1), \tag{19}$$

$$\mu_2(\rho_2;\rho_1)=\mu_3(\rho_3;\rho_1,\rho_2)=\mu_3(0;\rho_1,\rho_2). \tag{20}$$

Since ρ_3 is the density of a dilute system μ_3 can be evaluated at zero density. It is the binding energy of an atom in the effective potentials provided by the carbon substrate, first and second layers. We thus have two equations to be solved self consistently for ρ_1 and ρ_2. In the 2D approximation the chemical potentials are easily calculated and the two equations can be readily solved interactively. We find that the density at which the second layer completes is $\rho_2 = 0.08\ \text{Å}^{-2}$, and at this density the first layer density has increased by 4% to 0.115 Å^{-2}. The density of total coverage is thus 0.195 Å^{-2}. The experimental range is 0.204 to 0.212 Å^{-2}.[30] Our result is approximately 5% below the lowest experimental values. Thus for both the first and second layers the 2D approximation yields completion densities which are somewhat low. The density of the first layer has increased by about 4% which is in the range of experimental values. We can compare the density profiles of the first layer in the presence of a dilute second layer and in the presence of the completed second layer. We find that the position of the maximum is unchanged, but that the height has increased by 6% and the width has decreased by 8%. Clearly the first layer has been compressed by the completed second layer.

There has been some discussion in the literature as to whether the second layer crystallizes into an incommensurate solid just before completion or whether it requires the compression provided by a partly full third layer. Within the framework of our 2D model the second layer completes at a density of 0.08 Å^{-2}. This is well above the freezing density of 2D helium, which is 0.0678 Å^{-2}. We can however make a somewhat stronger statement. We notice from Table IV that the melting and freezing densities of 2D helium and the first layer film are very close. We expect on this basis that the melting and freezing densities of the second layer will be extremely close to these of the first layer. While the density profile of the second layer is 50% wider than that of the first however it is still so narrow that the configurations of the second layer must be very close to those of the 2D system. We thus have very good reason to believe that the second layer will crystallize before completion. This qualitative argument has been confirmed by explicit calculations. We find at a density of 0.08 Å^{-2} that the crystal phase has a lower energy than the fluid phase. These are GFMC results, the energy difference being approximately 0.4 K. This is in agreement with the neutron-scattering data.[31]

On the basis of our work we cannot make any firm prediction as to whether the third layers will crystallize at or before completion. Experimentally the third layer[2] completes at a lower density (0.07 Å^{-2}) than the second. This density is now very close to the melting density of both the 2D and the first layer. We should also point out that the density profile of the third layer is approximately twice as wide as that of the first layer. This will lead to a significant lowering of the energies of both the fluid and solid phases (if one exits) thus making it difficult to predict the freezing density of the layer. While it is plausible that the third layer remains fluid at completion we have no strong argument to support that conclusion.

It is interesting to note that under our assumptions the chemical potential of the dilute third layer is -8.5 K. This can be compared with the chemical potential of bulk 3D liquid helium which, with our two-body potential and no three-body potential, is -7.2 K. These values can be contrasted with the values of the chemical potential of the dilute first and second layers which are approximately -140 and -25 K, respectively. The chemical potential of the third layer will slowly rise as the layer fills and reaches completion. Its value at that density must be close to, but below that of the bulk fluid. We can thus conclude that since four more layers can be observed at low temperatures each of these layers must lead to a very small increments in the chemical potential of the system. This appears to be a very subtle effect and would be very difficult to treat with precision by our methods; indeed the variational methods developed by Clements *et al.*[6] may well be more suitable.

These values of the chemical potentials of each dilute layer merely reflect the strength of the attractive potentials seen by the atoms in the dilute layer. For the first layer the atoms merely see the potential of the carbon substrate: this

has a value of approximately -180 K. The atoms in the dilute second layer see a much weaker potential of approximately -50 K. It is interesting to note that this has approximately equal contributions of about -25 K from the distant carbon substrate and from the dense first layer. The atoms in the third layer see only a very weak carbon potential, -5 K, a smaller contribution from the dense first layer, -2 K, and the largest contribution from the second layer, -15 K. These values are at the minimum of the total potential; the total depth at the minimum being -22 K. This value is close to the minimum of the two-layer model potential used by Clements *et al.*[9]

In Fig. 1 we show the single-particle wave functions for the three layers. The wave function for the first layer is calculated taking into account both the carbon substrate and the completed second layer. As we have noted the second layer compresses the wave function and density profile of the first layer. They indeed show little overlap and the first and second layers are tightly bound. Thus for these two layers we expect our approximations to work well. However the third layer is a good deal wider which tells us that it is unlikely that our 2D approximations will be as accurate if applied to this layer. However to determine the densities ρ_1 and ρ_2 at which this layer begins to form does not require us to make any approximations about how tightly it is bound.

VI. DISCUSSION

We have shown, within the framework of a smooth substrate model, that one can accurately calculate the properties of the first two layers of helium on graphite. In the model these layers are well separated and very tightly bound to the substrate. As the density in each layer increases, condensation into a uniform self-bound liquid will take place at about 0.04 Å^{-2}, and crystallization into a triangular lattice will occur at 0.07 Å^{-2}. We are able to compute the completion densities of both the first and second layers and find agreement, to within a few percent, with the experimental values. Beyond the second layer our methods may be less useful.

The major defect in our model is the absence of a realistic substrate. Not only have we removed the basic periodicity of the graphite lattice we have also eliminated any irregularities, such as steps and islands on the surface. In our model at low densities nearly two-dimensional clusters will form which will increase in size and eventually percolate to form a connected fluid film. On a realistic substrate condensation may well take place preferentially on step edges and other irregularities. Moreover the condensation into clusters has to compete with the formation of a commensurate phase. These considerations are of course most important for the first layer where the helium atoms experience only the bare graphite potential. In the second layer the periodicity of the graphite potential is quite small and the irregularities of the graphite surface may well be smoothed out by the dense first layer. Nevertheless the second layer atoms experience the periodic potential provided by the dense triangular lattice of the first layer. For this layer too, condensation has to compete with the formation of a commensurate phase.

Superfluidity has been seen in the second layer.[3] The highest density, 0.07 Å^{-2}, at which it has been detected is approximately the density at which the layer will start to freeze into a triangular lattice. The lowest density, 0.05 Å^{-2}, is definitely above the density at which a homogeneous film will form in our smooth substrate model. This discrepancy may be due to the irregularities on the surface leading to preferential condensation on steps and thus delaying the formation of a homogeneous, or at least extended fluid film. Alternatively it may be due to the presence of a commensurate phase. The surface structure is clearly important to understanding the behavior of the first and second layer films on graphite. For this reason we plan to explore the topic with both variational and GFMC calculations.

ACKNOWLEDGMENTS

We thank William Magro for providing the value of the chemical potential in the dilute second layer obtained from a path-integral simulation. We also thank James Porter for evaluating the static lattice sum for the Axelrod-Teller potential. This work was partially supported by the National Science Foundation under Grant No. DMR 9200409, and by the Office of Naval Research Grant No. N00014-96-1-1-1057.

APPENDIX

We can readily find a potential $V_{\max}(z)$ which is larger than V_E for all $\underline{x,y}$. Similarly we can find $V_{\min}(z)$ which is a lower bound to V_E for all (x,y). It is then straightforward to prove that the lowest eigenvalue of V_E must be between the lowest eigenvalues of $V_{\max}(z)$ and $V_{\min}(z)$. The upper bound $V_{\max}(z)$ occurs when the coordinates x,y are held fixed above a helium atom in the crystalline layer. The lower bound $V_{\min}(z)$ occurs when x,y are held fixed at the center of one of the triangles of the lattice.

First we show that if $V(r) \leqslant V_{\max}(r)$, for all r, then $E \leqslant E_{\max}$. Let $\Psi_{\max}(r)$ denote the normalized ground-state wave function for the potential $V_{\max}(r)$, then

$$E_{\max} = \int d^3r\ \Psi^{\dagger}_{\max}(r)[T + V_{\max}(r)]\Psi_{\max}, \qquad \text{(A1)}$$

where T is the three-dimensional kinetic energy operator, and the symbol † indicates complex conjugation. If we choose $\Psi_{\max}(r)$ as a variational wave function for the Hamiltonian $[T+V(r)]$, then from the variational theorem we know that

$$E \leqslant \int d^3r\ \Psi^{\dagger}_{\max}(r)[T + V(r)]\Psi_{\max}(r). \qquad \text{(A2)}$$

Subtracting Eq. (A1) from Eq. (A2) we find that

$$E - E_{\max} \leqslant \int d^3\underline{r}\ \Psi^{\dagger}_{\max}[V(r) - V_{\max}(r)]\Psi_{\max}, \qquad \text{(A3)}$$

and since $V(r) \leqslant V_{\max}(r)$ for all r,

$$\int d^3r\ \Psi^{\dagger}_{\max}(\underline{r})[V(r) - V_{\max}(r)]\Psi_{\max}(r)$$

$$\equiv \int d^3r[V(r) - V_{\max}(r)]|\Psi_{\max}(r)|^2 \leqslant 0. \qquad \text{(A4)}$$

From Eqs. (A3) and (A4) we conclude that $E \leqslant E_{\max}$. By a similar argument we can show that if $V_{\min}(r) \leqslant V(r)$ the $E_{\min} \leqslant E$. This proves our assertion. Now since $V_{\max}(r)$ and $V_{\min}(r)$ depend only on z it follows that $E_{\max}$ and $E_{\min}$ are the ground-state energies of the corresponding one-dimensional eigenvalue problems. These one-dimensional eigenvalue problems are easily solved numerically and we therefore do not need to find the lowest eigenvalue of the full three-dimensional potential V_E.

[1] *Phase Transitions in Surface Films*, edited by J. G. Dash and J. Ruvalds (Plenum, New York, 1980); *Phase Transitions in Surface Films 2*, edited by H. Taub, G. Torzo, H. J. Lauter, and S. C. Fain, Jr. (Plenum, New York, 1991); *Excitations in Two and Three Dimensional Quantum Fluids*, edited by A. F. G. Wyatt and H. G. Lauter (Plenum, New York, 1991).

[2] D. S. Greywall and P. A. Busch, Phys. Rev. Lett. **67**, 3535 (1991); D. S. Greywall, Phys. Rev. B **47**, 309 (1993); G. Zimmerli, G. Mistura, and M. W. H. Chan, Phys. Rev. Lett. **68**, 60 (1992).

[3] P. A. Crowell and J. D. Reppy, Phys. Rev. B **53**, 2701 (1996).

[4] C. E. Campbell, F. J. Milford, A. D. Novaco, and M. Schick, Phys. Rev. A **6**, 1648 (1972).

[5] P. A. Whitlock, G. V. Chester, and M. H. Kalos, Phys. Rev. B **38**, 2418 (1988).

[6] B. E. Clements, E. Krotscheck, H. Lauter, and M. Saarela, in *Condensed Matter Theories*, edited by J. W. Clark, K. A. Shoaib, and A. Sadiq (Nova Science, Commack, New York, 1994), Vol. 9, p. 3.

[7] K. A. Gernoth, J. W. Clark, and M. L. Ristig, in *Condensed Matter Theories*, edited by M. Casas, M. de Llano, J. Navarraw, and A. Palls (Nova Science, Commack, New York, 1995), Vol. 10, p. 91.

[8] M. Saarela, B. E. Clements, E. Krotscheck, and F. V. Kusmartsev (Ref. 7), p. 119.

[9] B. E. Clements, J. L. Epstein, E. Krotscheck, and M. Saarela, Phys. Rev. B **48**, 7450 (1993); B. E. Clements, H. Forbert, E. Krotscheck, and M. Saarela, J. Low Temp. Phys. **95**, 849 (1994).

[10] N. Pavloff and J. Treiner, J. Low Temp. Phys. **83**, 331 (1991).

[11] J. Dupont-Roc, M. Himbert, N. Pavloff, and J. Treiner, J. Low Temp. Phys. **81**, 31 (1990).

[12] E. Krotscheck (Ref. 7), p. 13.

[13] K. E. Schmidt and D. M. Ceperley, in *Monte Carlo Methods in Condensed Matter Physics*, Topics in Modern Physics, Vol. 71, edited by K. Binder (Springer-Verlag, Berlin, 1991), pp. 205–245.

[14] P. A. Whitlock, D. M. Ceperley, G. V. Chester, and M. H. Kalos, Phys. Rev. B **19**, 5598 (1979).

[15] R. A. Aziz, V. P. S. Nain, J. S. Carley, W. L. Taylor, and G. T. McConville, J. Chem. Phys. **70**, 4330 (1979).

[16] M. H. Kalos, M. A. Lee, P. A. Whitlock, and G. V. Chester, Phys. Rev. B **24**, 115 (1981).

[17] W. E. Carlos and M. W. Cole, Surf. Sci. **91**, 339 (1980).

[18] E. V. Haynsworth and K. Goldberg, in *Handbook of Mathematical Functions*, edited by M. Abramowitz and I. A. Stegun (Dover, New York, 1970), Chap. 23.

[19] T. MacFarland, S. A. Vitiello, L. Reatto, G. V. Chester, and M. Kalos, Phys. Rev. B **50**, 13 577 (1994).

[20] K. E. Schmidt, M. H. Kalos, M. A. Lee, and G. V. Chester, Phys. Rev. Lett. **45**, 573 (1980); K. E. Schmidt, M. A. Lee, M. H. Kalos, and G. V. Chester, *ibid.* **47**, 807 (1981).

[21] B. Brami, F. July, and C. Lhuillier, J. Low Temp. Phys. **94**, 63 (1994).

[22] E. Cheng, M. W. Cole, and P. B. Shaw, J. Low Temp. Phys. **82**, 49 (1991).

[23] We have carried out both variational and GFMC calculations at densities of 0.11 and 0.12 Å^{-2} so that our chemical potential calculation extends to the density of first layer completion. The polynomial fit Eq. (10) extrapolates very accurately to these densities.

[24] K. Carneiro, L. Passell, W. Thomlinson, and H. Taub, Phys. Rev. B **24**, 1170 (1981); D. S. Greywall and P. A. Busch, Phys. Rev. Lett. **67**, 1007 (1991).

[25] R. A. Aziz, M. J. Slaman, A. Koide, A. R. Allnatt, and W. J. Meath, Mol. Phys. **77**, 321 (1992); A. R. Janzen and R. A. Aziz, J. Chem. Phys. **107**, 914 (1997).

[26] R. D. Murphy and J. A. Barker, Phys. Rev. A **3**, 1037 (1971).

[27] In the high-density range of the film we evaluated the contribution of the three-body potential to the total energy by performing a static lattice sum. In this range the lattice is nearly harmonic and we therefore expect that static lattice approximation to be quite accurate.

[28] A. D. Novaco and C. E. Campbell, Phys. Rev. B **11**, 2525 (1975).

[29] C. E. Campbell and M. Schick, Phys. Rev. A **3**, 691 (1971).

[30] D. S. Greywall, Phys. Rev. B **47**, 309 (1992); H. J. Lauter, H. Godfrin, H. Wiechert, G. Zimmerli, G. Mistura, and M. W. H. Chan, Phys. Rev. Lett. **68**, 60 (1992).

[31] H. J. Lauter, H. P. Schildberg, H. Goldfrin, H. Wiechert, and R. Haensel, Can. J. Phys. **65**, 1435 (1987).